Available online at www.sciencedirect.com
ScienceDirect
Journal of Sound and Vibration 323 (2009) 495–514
JOURNAL OF SOUND AND VIBRATION
www.elsevier.com/locate/jsvi

Multi-objective optimization of piezo actuator placement and sizing using genetic algorithm

K.D. Dhuri, P. Seshu*

Department of Mechanical Engineering, Indian Institute of Technology Bombay, Powai, Mumbai 400 076, India

Received 17 October 2007; received in revised form 2 January 2009; accepted 6 January 2009
Handling Editor: J. Lam
Available online 25 February 2009

Abstract

Sizing and placement of piezoelectric sensors and actuators (S/As) for active vibration control of flexible structures is commonly based on maximum control effectiveness. Mounting of piezos changes the natural frequencies of existing structure, which would have been designed to have a certain natural frequency spectrum in relation to the disturbance excitation. In the event of failure of the active system, natural frequencies of the structure with piezos (now rendered passive) become significant. Therefore minimal change in natural frequency along with good controllability should be design consideration while deciding sizing and placement of actuators. Multi-objective genetic algorithm is shown to be useful for optimization of placement and sizing of piezo actuators for such problems. Optimal S/As sizing and locations have been found out for stationary and rotating cantilever beams with multiple sensors/actuators.

1. Introduction

Active vibration control of flexible structures using piezoelectric sensors/actuators has been a major research topic during past two decades. It is imperative to have appropriately located piezoelectric sensors and actuators (S/As) of suitable size and to ensure the maximum effectiveness for vibration control. Therefore the efforts have been mainly concentrated on finding the optimal size and location of the S/As. Optimal locations of piezoelectric actuators for active vibration control of cantilever beam is first addressed by Crawley and de Luis [1]. Baz and Poh [2] solved the problem of location optimization of an actuator with pre-selected size. Devasia et al. [3] analyzed the problem of placement and sizing of distributed piezoelectric actuators to achieve effective vibration control. Passive damping and LQR-based optimization has been recommended. Dhingra and Lee [4] addressed the influence of S/A locations and feedback gains on the optimum design of actively controlled structures. Moheimani and Ryall [5] have introduced modal and spatial controllability notion, based on H_2 norm while choosing optimal locations for piezo patches.

Hac and Liu [6] have proposed a criterion for S/As placement to achieve a balance between the importance of controlling/observing lower order and higher order modes. Kang et al. [7] studied optimal placement of

*Corresponding author. Tel.: +91 22 25767534; fax: +91 22 25726875.
E-mail address: seshu@iitb.ac.in (P. Seshu).

0022-460X/$ - see front matter © 2009 Elsevier Ltd. All rights reserved.
doi:10.1016/j.jsv.2009.01.007

sensor/actuator for vibration control of laminated beams using structural damping index (*product of modal damping and mode shape function*).

A few studies have used genetic algorithm (GA) for finding out the optimal sizing, locations of piezos and other vibration control related parameters. Rao et al. [8] have used GA for identifying piezo actuator locations for actively controlled structures. Yang et al. [9] have developed an integer–real-encoded GA for identifying optimal sizing and location of piezoelectric patches as well as the optimal feedback control gains. Sheng and Kapania [10] have used GA for finding the optimal locations of piezoelectric actuators for ensuring high surface accuracy of a telescope mirror.

Practical problems are often characterized by several non-commensurable and competing measures of performance, thus leading to multi-objective optimization problems. Dhingra and Lee [11] have developed multi-objective (structure and control optimization), hybrid optimization model based on GA and gradient-based search techniques for actively controlled flexible structures. Hau et al. [12] used multi-objective genetic algorithm (MOGA) for active vibration control of rotating flexible arm using active constrained layer damping treatment. The objectives were to minimize total treatment weight, the control voltage and the tip deflection and to maximize the passive damping characteristics. Padula et al. [13] reviewed optimization activities for sensor and actuator placement till 1999. Frecker [14] enumerated several optimization studies in smart structures during 1999–2003. Maximum deflection, minimum power consumption and maximum controllability were some of the objective functions of the studies.In above studies, for optimization of actuator sizing and placement, different cost functions and performance measures have been used. Most of the studies (e.g. [6,15]) have maximized the controllability. Few studies have used a quadratic cost function taking into account the measurement error and control energy [11,16].

Thus, in most of these studies, optimization is based on control effectiveness consideration. But, the piezoelectric S/As, while providing active control, modify the inherent stiffness/mass properties of the parent structure. In rotating beams, the additional mass due to piezo patch actuators contributes to the centrifugal stiffening force. The parent structure is originally designed to have certain natural frequency (NF) spectrum vis-à-vis disturbance excitation. *In the event of failure of the active system*, *dynamics of structure with piezos* (*now rendered passive*) *will therefore become significant.* Hence, it is imperative to mount piezo patches at such locations, which will cause possibly minimal change in the natural frequencies of parent structure yet possess significant control effectiveness. Authors have recently carried out an exhaustive study [17], which gives such locations for a *single pair of S/A* by exhaustive search. The study identifies the piezo mounting sizing and locations considering first four modes for stationary and rotating cantilever beam. But such an exhaustive study becomes computationally intensive when number of piezo patches and other design variables increases. In this study, multi-objective optimization problem is formulated using GA. Maximization of controllability and minimization of NF changes are the objective functions. The finite element method (FEM) is employed to model the flexible beam.

2. Dynamic modeling of a rotating beam with piezo actuators

Consider the rotating beam shown in Fig. 1. Consider an inertial frame—**R**(**OXYZ**) and a moving frame—$\mathbf{R}_0$ ($\mathbf{X}_0\mathbf{Y}_0\mathbf{Z}_0$) which is attached to the beam, assumed to be rotating about the $\mathbf{Y}_0$-axis with constant speed Ω (rad/s) with respect to inertial frame. Flexural vibration in $\mathbf{X}_0\mathbf{Y}_0$-plane is of interest. The detailed expression of the potential and kinetic energies and then derivation of equation of motion using Lagrange's equation are given in Ref. [17].

2.1. Finite element modeling

The standard 2-noded beam element [18] having 3 dof at each node as shown in Fig. 2, is used for modeling the system. u, v and θ_z are the deformations in axial, transverse direction and rotation, respectively. The total stiffness consists of standard beam stiffness due to substrate beam and piezo and the geometric stiffness matrix pertaining to the effects of rotation. The standard stiffness matrix, $[\mathbf{k}_E]$ of the element is modified for present study. For an element representing the substrate beam with piezo patches, flexural rigidity is given by $EI = E_bI_b + 2E_pI_p$ and for other element, $EI = E_bI_b$; where I_p is the area moment of inertia of each piezo patch

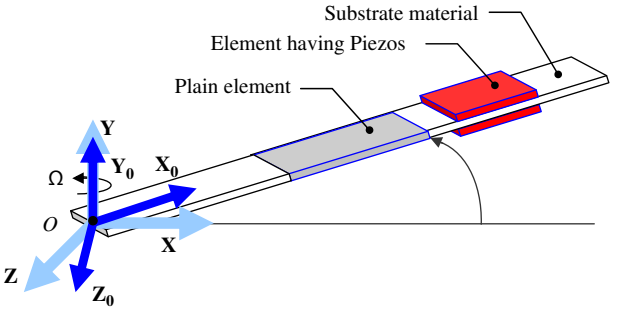

Fig. 1. Rotating cantilever beam with piezos.

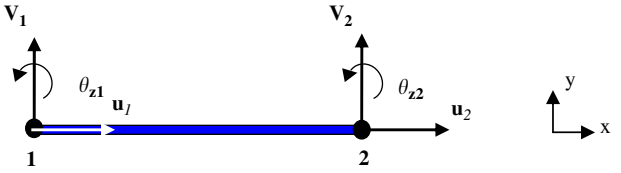

Fig. 2. Beam element.

about mid-plane of the substrate beam. Similarly, for an element representing substrate beam with piezo patches, EA in the stiffness matrix is calculated for equivalent section.

2.1.1. Geometric stiffness matrix due to rotation

The additional stiffness due to presence of axial stress σ_x^0 caused by rotation is given by

$$[\mathbf{k}_G] = \int_0^{l_e} [\mathbf{G}]^T [\sigma_x^0][\mathbf{G}] A \, \mathrm{d}x \tag{1}$$

where G is defined by

$$\left\{\frac{\partial v}{\partial x}\right\} = [\mathbf{G}]\{q_e\} \tag{2}$$

where $\{q_e\}$ consists of nodal dof. The stresses incurred in the cantilever beam due to rotation are approximated from a quasi-static force analysis, wherein the displacements and internal forces are calculated due to inertial and external forces on the system [19].

2.1.2. Mass, Coriolis, rotational stiffness matrices and load vector

The standard consistent mass matrix [20] is modified for the present study considering the effect of piezoelectric patches on the lines of stiffness matrix, as discussed earlier in Section 2.1. From equation of motion, after expressing u and v in terms of nodal coordinates using shape functions, Coriolis $[\mathbf{c}]$, rotational stiffness $[\mathbf{k}_R]$ matrices and load vectors $\mathbf{f}_1(\Omega^2)$ can be obtained. The detailed expressions are given in Ref. [17].

2.1.3. Piezoelectric patch modelling

In this study, electrical dof is not explicitly considered for the finite element, whereas electromechanical coupling has been modeled as discussed in this section. The bending moment produced from the ith piezoceramic actuator bonded on flexible link surface due to the control input voltage $V_{Ci}(t)$ can be obtained by considering force equilibrium in the axial direction [21]. The moment M_i applied by the piezo actuator on the flexible link about its neutral axis is determined by

$$M_i = -\varepsilon_p E_p t_p b[t_p/2 + t_b/2] = \hat{c}_i V_{Ci}(t) \tag{3}$$

where t and b are thickness and width, respectively. ε_p is the strain induced in the piezoceramic due to voltage applied across it, which is given by $\varepsilon_p = d_{31}V_{Ci}(t)/t_p$, where d_{31} is the piezoelectric strain constant. The constant $\hat{c}_i$ implies the bending moment per unit applied voltage, which is calculated from the geometric and material properties of the substrate link and piezo patch combination [22]. Control force/moment vector, $f_2(V_C)$ is computed using Eq. (3).

2.1.4. Final equations after assembly

The final equation for the structure after assembly of all the elements is of the form,

$$[\mathbf{M}]\{\ddot{\delta}\} + [\mathbf{C}]\{\dot{\delta}\} + [\mathbf{K}]\{\delta\} = \{\mathbf{F}_1(\Omega^2)\} + \{\mathbf{F}_2(V_C)\} \tag{4}$$

where $[\mathbf{M}]$, $[\mathbf{C}]$, $[\mathbf{K}] = [\mathbf{K}_E] + [\mathbf{K}_G] + [\mathbf{K}_R]$, $\mathbf{F}_1(\Omega^2)$ and $\mathbf{F}_2(V_C)$ are the mass, damping, stiffness matrices and force vectors due to rotation and control moments. The eigen value problem can be written as

$$[\mathbf{M}]\{\ddot{\delta}\} + [\mathbf{C}]\{\dot{\delta}\} + [\mathbf{K}]\{\delta\} = 0 \tag{5}$$

In the above equation, $[\mathbf{M}]$ and $[\mathbf{K}]$ are symmetric and positive definite and $[\mathbf{C}]$ is skew-symmetric. The Coriolis matrix is only proportional to the angular velocity, whereas the geometric stiffness and rotational stiffness matrices are proportional to the square of the angular velocity and so will have greater influence on the system natural frequencies than the Coriolis matrix. Therefore the effect of $[\mathbf{C}]$ matrix is negligible [23]. Also, to speed up the computation consistent mass matrix is replaced by diagonal lumped mass matrix [18].

$$[\mathbf{M}] = m[1/2 \;\; 1/2 \;\; l_e^2/24 \;\; 1/2 \;\; 1/2 \;\; l_e^2/24] \tag{6}$$

where, m is the total mass of the element. The m of the element, whose base structure is covered by piezoelectric patches on both sides is given by $m = (\rho_b A_b + 2\rho_p A_p)l_e$. Above formulation is implemented in MATLAB®7 [24]. Subspace iteration approach [20] has been used for solving the eigen value problem to get the natural frequencies and mode shapes.

3. Controller

In this study, proportional and derivative (PD) controller is used for actively controlling the vibration of stationary/rotating cantilever beam. Applying a PD control law, the control voltage calculated for the ith piezo actuator V_{Ci} from corresponding piezo sensor voltage V_{Si} is given by

$$V_{Ci} = -K_p V_{Si} - K_d \, \mathrm{d}V_{Si}/\mathrm{d}t \tag{7}$$

where K_p and K_d are the PD gain, respectively. The voltage of the ith sensor, V_S is calculated from [25],

$$V_{Si} = \frac{-k_{31}^2 D_d b}{g_{31}\hat{C}} \sum_{i=i_s}^{i_f} f(x)v'' \, \mathrm{d}x \tag{8}$$

where D_d is the distance from the beam neutral axis to the sensor surface and $f(x)$ is the distribution shape function of the sensor. The sensor is mounted between elements i_s and i_f. Also, k_{31} is electro-mechanical coupling factor and g_{31} is piezoelectric voltage constant and $\hat{C}$ is the capacitance of sensor. The controller is implemented using MATLAB® 7.

4. Modal controllability

The controllability of a system having n_p piezo actuators controlling first n mode shapes is briefly described below [26]. After carrying out modal analysis and considering n mode shapes, the system dynamics equations can be represented in state space as

$$\{\dot{\mathbf{X}}\} = [\mathbf{A}]\{X\} + [\mathbf{B}]\{U\} \tag{9}$$

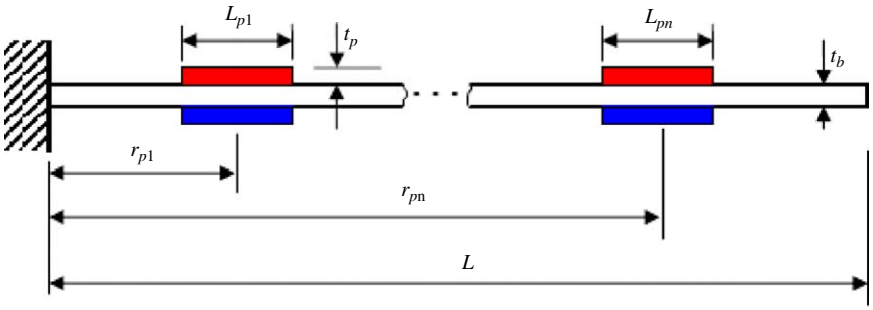

Fig. 3. Cantilever beam with piezo patches on both sides.

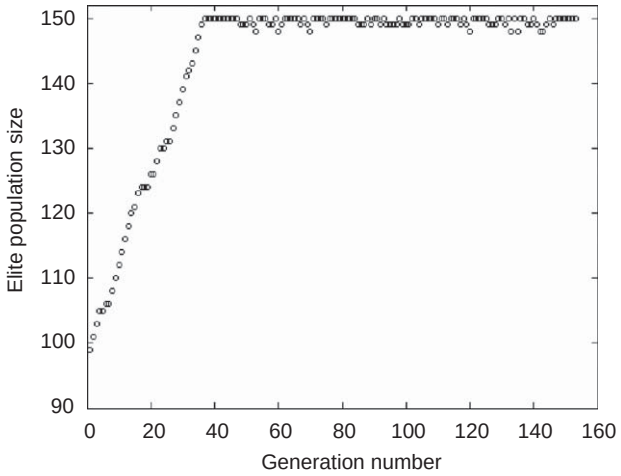

Fig. 4. Growth of elite population size for a beam with two collocated piezo S/A pairs.

Table 1
System properties of cantilever beam with piezo.

Attribute	Beam (aluminum)	Piezo patch (PZT) [31]
Geometry ($L \times b \times t$) (mm)	$300 \times 25 \times 0.5$	$L_p \times 25 \times 0.35$
Modulus of elasticity, E (N/m^2)	60×10^9	62×10^9
Density, ρ (kg/m^3)	2400	7500
Strain coefficient, d_{31} (m/V)	–	247×10^{-12}
Electric field (V/mm)	–	1000

Table 2
Comparison of first five natural frequencies (Hz) of stationary and rotating (300 rev/min) cantilever beam with and without piezo patches.

Mode number	Stationary plain beam	Stationary beam with piezo	Rotating plain beam	Rotating beam with piezo
1	4.49	3.11	7.04	6.23
2	28.12	28.46	30.87	33.61
3	78.74	81.77	81.52	87.82
4	154.30	166.18	157.19	175.64
5	255.06	257.16	258.02	266.33

where state vector, $[\mathbf{X}]^T = \{q^T, \dot{q}^T\}$, with $q = \{q_1, q_2, \ldots, q_n\}$ and $\dot{q} = \{q_i, \dot{q}_2, \ldots, \dot{q}_n\}$, q_i are the generalized modal coordinates and electric potential vector is

$$[\mathbf{U}] = \{v_{a1}, v_{a2}, \ldots, v_{an_p}\}^T \tag{10}$$

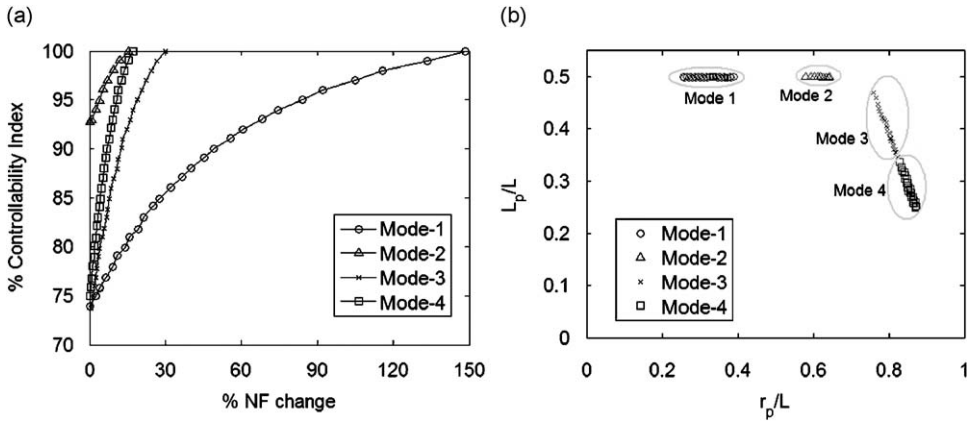

Fig. 5. Pareto optimal solution for stationary cantilever beam with a pair of collocated S/A: (a) PO objective sets and (b) PO solutions.

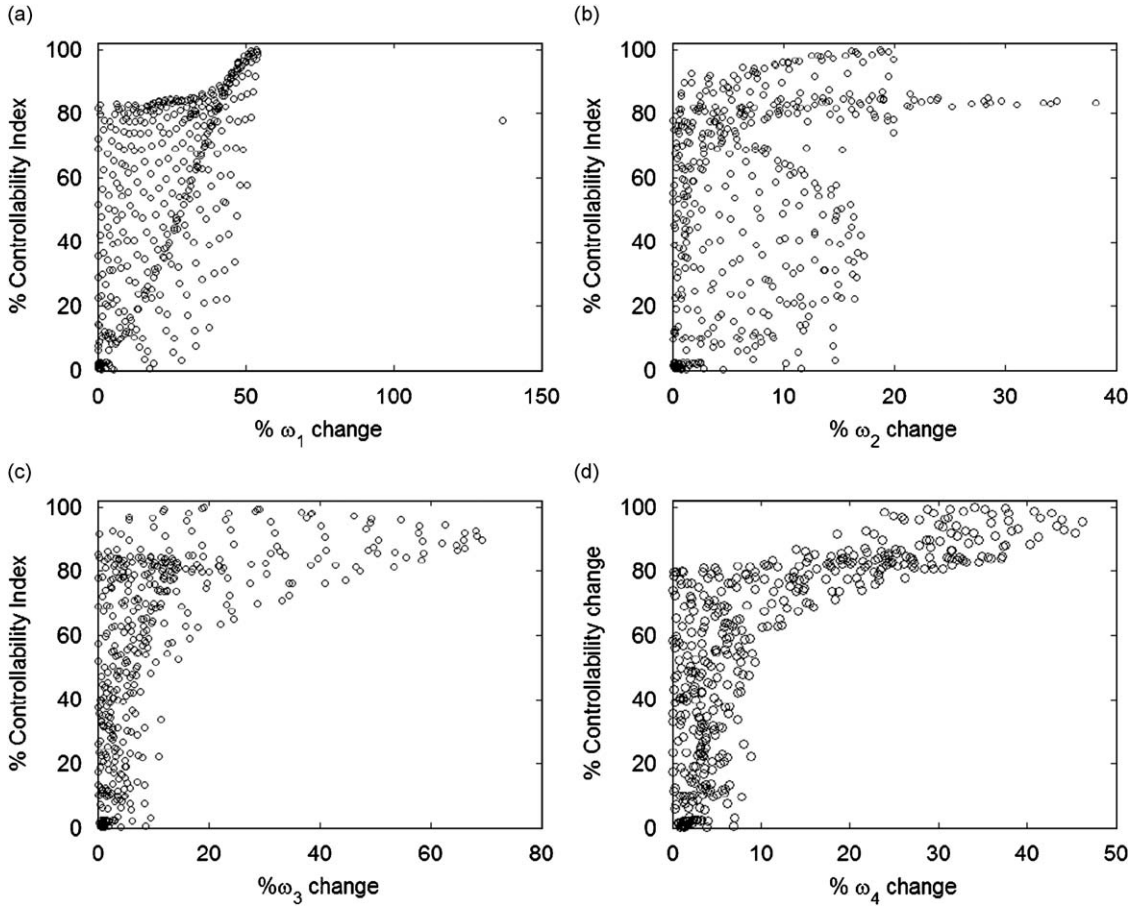

Fig. 6. Projection of Pareto optimal objective set on natural frequency change and controllability for stationary cantilever beam with a pair of collocated S/A for first four modes: (a) mode 1, (b) mode 2, (c) mode 3 and (d) mode 4.

where v_{ai} is the electric potential provided to the ith piezoelectric actuator. The system matrices [**A**] and [**B**] are given by

$$[\mathbf{A}] = \begin{bmatrix} 0 & I \\ -\omega^2 & 0 \end{bmatrix} \tag{11}$$

$$[\mathbf{B}] = \begin{bmatrix} 0 \\ B_a \end{bmatrix}, \quad \text{where } B_a = \begin{bmatrix} B^1_{a1} & B^1_{a2} & \dots & B^1_{an_p} \\ B^2_{a1} & B^2_{a2} & \dots & B^2_{an_p} \\ \vdots & \vdots & \vdots & \vdots \\ B^n_{a1} & B^n_{a2} & \dots & B^n_{an_p} \end{bmatrix} \quad \text{with } B^j_{ap} = [\phi'_j(x_{pe}) - \phi'_j(x_{ps})] \tag{12}$$

$\phi'_j(x_{ps})$ and $\phi'_j(x_{pe})$ are the slopes of the jth displacement mode shape i.e. rotation dofs of the nodes corresponding to end positions of the piezo in jth mode. Thus these values are readily available from

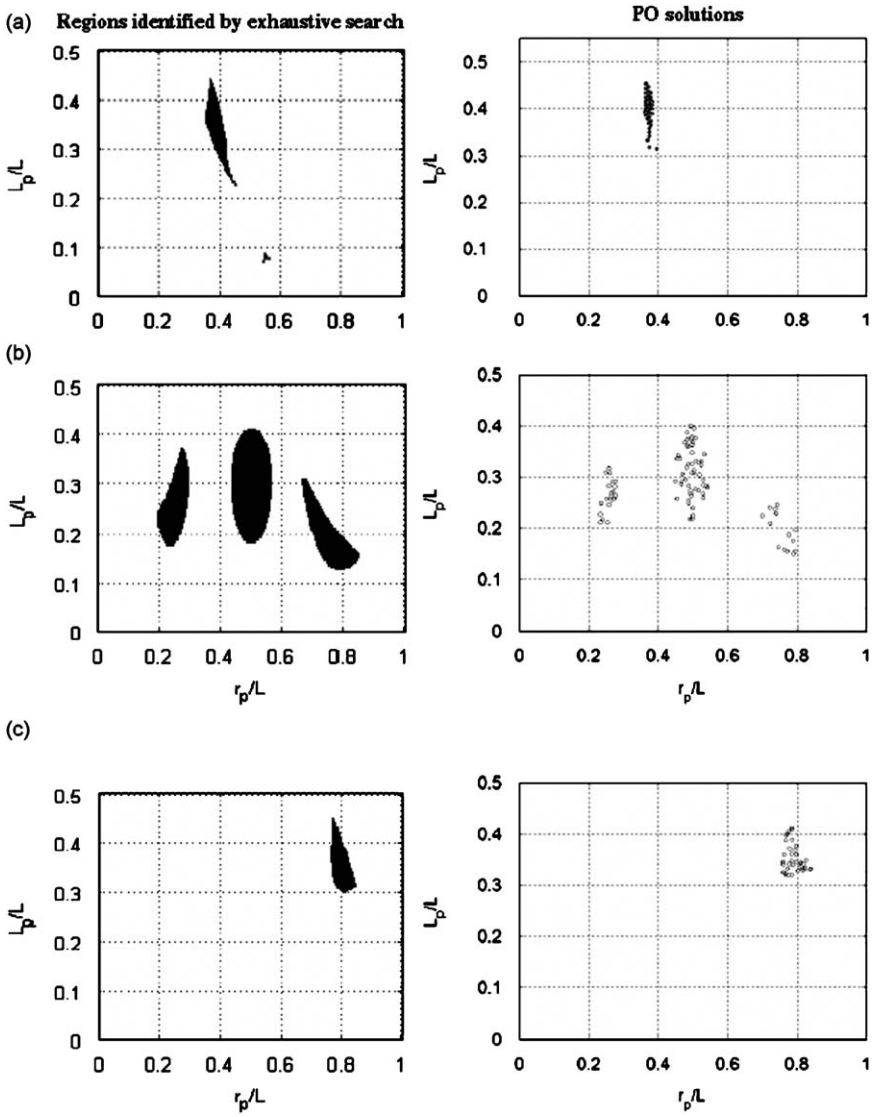

Fig. 7. Pareto optimal solution for stationary cantilever beam with a pair of collocated S/A for first four modes: (a) NF change < 10% and CI > 20%, (b) NF change < 40% and CI > 50% and (c) NF change < 70% and CI > 90%.

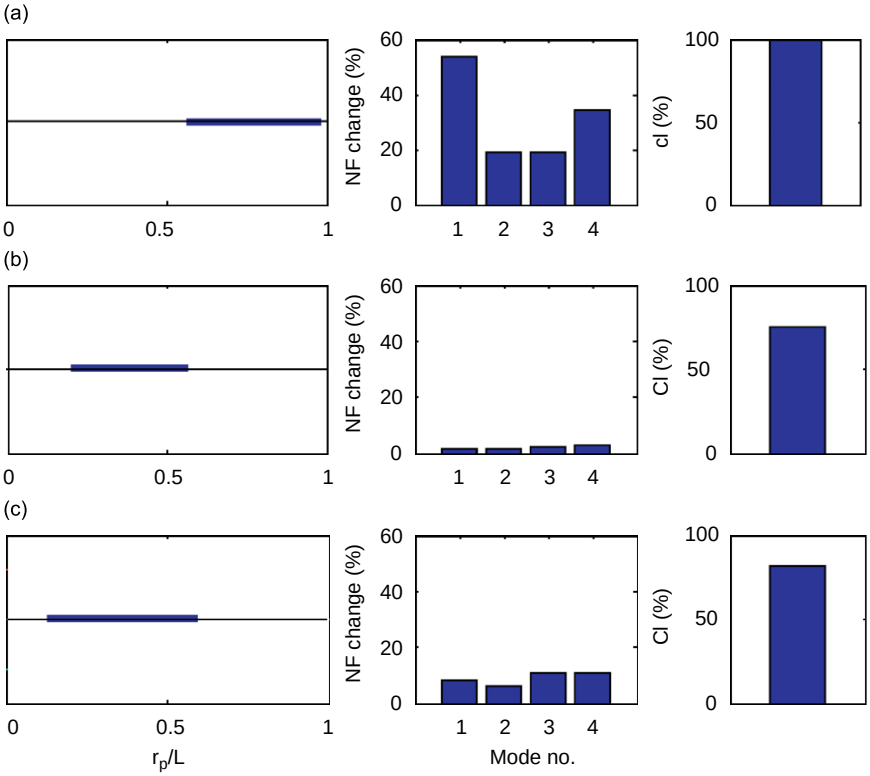

Fig. 8. Location and sizing of a piezo patch and first four natural frequency changes: (a) maximum controllability, (b) least NF change and (c) CI > 50% and lesser NF change.

the finite element simulation. Performing the singular value decomposition (SVD) of [**B**] we get the singular values

$$S = \begin{bmatrix} \sigma_1 & & \\ & \ddots & \\ & & \sigma_{n_p} \\ 0 & 0 & 0 \end{bmatrix}, \quad n_p < n \tag{13}$$

Magnitude of σ_i is a function of the location and size of piezoelectric actuators. The standard subroutine "SVD" available in MATLAB®7 has been used for SVD operation. For a single piezo patch, a singular value denotes the controllability index (CI) where as for multiple piezos, CI is calculated by [26]

$$\hat{\Omega} = \prod_{i=1}^{n_p} \sigma_i \tag{14}$$

The higher the CI, the lower the power consumption required for control i.e. the better the control effectiveness. Thus, in the current analysis, CI has been used as a measure of control effectiveness.

5. Optimization problem

5.1. Objective functions

As discussed earlier, the piezo sizing and locations should be such that those should give good controllability, yet minimal change in natural frequencies ($\Delta\omega_i/\omega_i$). This problem can be formulated in two different ways:

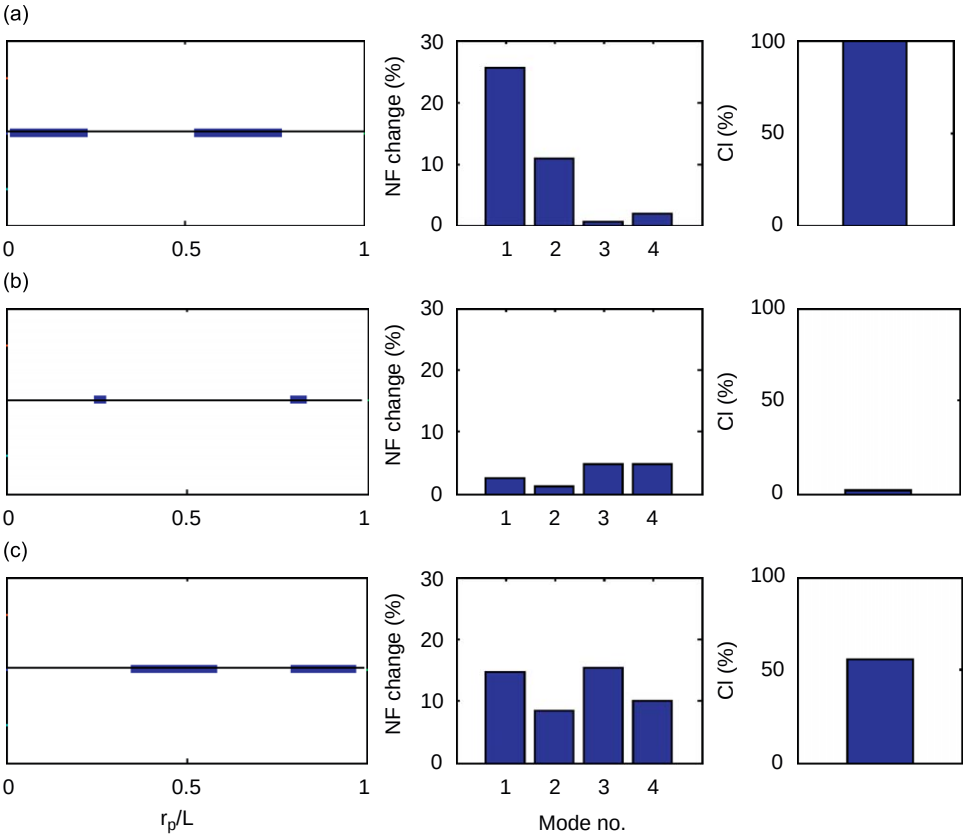

Fig. 9. Location and sizing of two piezo patches and first four natural frequency changes: (a) maximum controllability, (b) least NF change and (c) CI > 50% and moderate NF change.

(1) *A single-objective-optimization problem*: minimizing weighted sum of reciprocal of the CI and change in natural frequencies, under consideration. The objective function becomes

$$f = w_1 \frac{1}{\hat{\Omega}} + \sum_{i=1}^{n} w_{i+1} \frac{\Delta\omega_i}{\omega_i} \tag{15}$$

where $w_i$are the weighting coefficients which express the relative importance of the objectives and $n$is the number of modes considered.

(2) *Multi-objective optimization*: minimization of $(n+1)$ objective functions,

(a) Objective function 1: minimization of reciprocal of CI.

$$\text{Minimize} \quad f_1 = \frac{1}{\hat{\Omega}} \tag{16}$$

(b) Objective function $(i+1)$: minimization of change in ith NF.

$$\text{Minimize} \quad f_{i+1} = \frac{\Delta\omega_i}{\omega_i}, \quad i = 1, 2, \ldots, n \tag{17}$$

In most of the cases, deciding the weights in approach 1 is quite complex and it itself becomes an optimization problem. Also the problem of optimization of placement and sizing of piezoelectric patches, has no unique

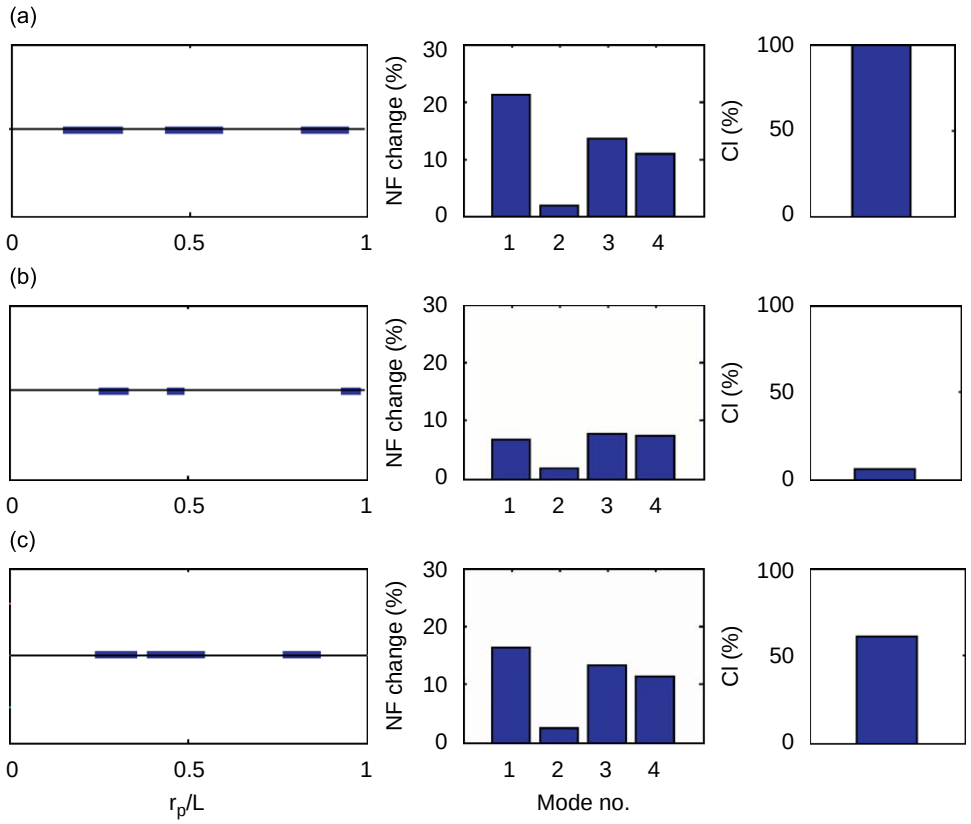

Fig. 10. Location and sizing of three piezo patches and first four natural frequency changes: (a) maximum controllability, (b) least NF change and (c) CI > 50% and lesser NF change.

solution, but a set of non-dominated, alternative solutions, known as the Pareto optimal (PO) set [27]. Therefore approach 2 is used in current study.

5.2. Design variables

The mounting of piezo patches is shown in Fig. 3. The size of the substrate beam is known. Length, thickness, width and location of the piezo patch are in general design variables. Out of these, thickness of commercially available piezoelectric patches comes in standard sizes. In this study, it is assumed as 0.35 mm. The width of the piezo patch is assumed equal to that of substrate beam. Thus, length of the piezo patch and its location on substrate beam are used as design parameters. The location is defined by the center of the piezo patch. These deign variables are normalized with respect to length of substrate beam. i.e. location, r_p/L and length, L_p/L.

5.3. Constraints

The normalized length of the piezo patch (L_p/L) is varied between 0.05 and 0.5. The lengths and locations of the piezo patches should be chosen such that those should not overlap and location should not go out of design domain ($L_p/2L$ to ($1–L_p/2L$)). It is also ensured that minimum gap between two patches is $0.01L$.

5.4. MOGA formulation

In this problem, the objective functions which involve controllability and NF computations are quite complex and gradient calculation of the objective functions is not straight forward. Therefore classical

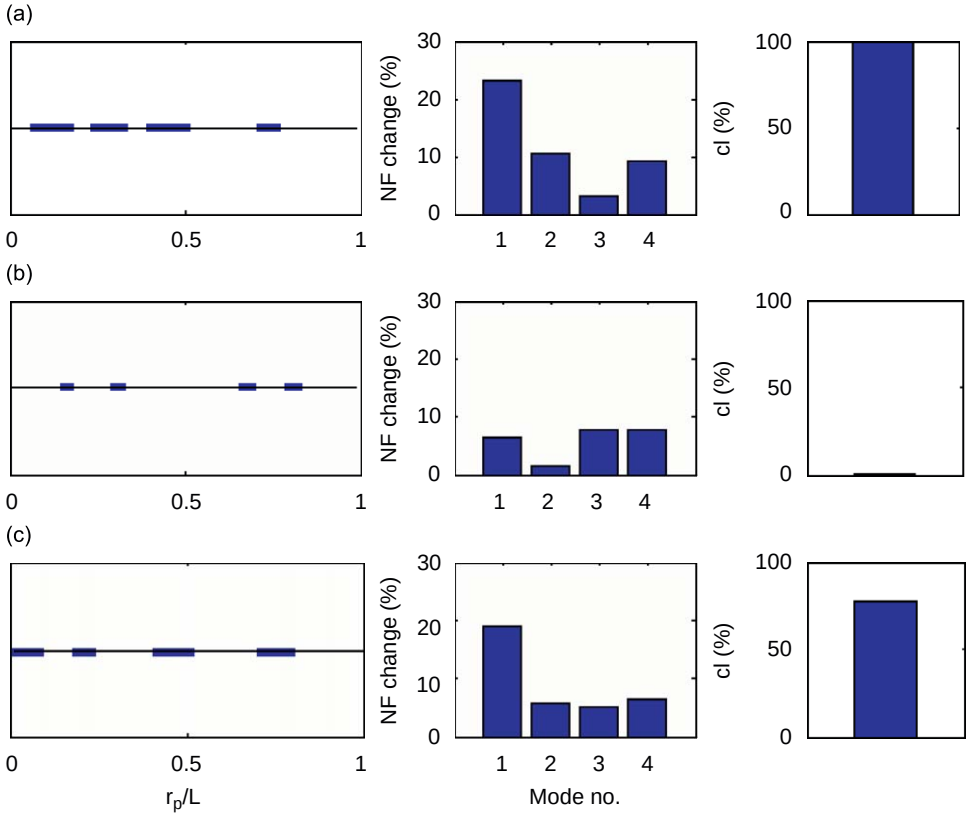

Fig. 11. Location and sizing of four piezo patches and first four natural frequency changes: (a) maximum controllability, (b) least NF change and (c) CI > 50% and lesser NF change.

optimization methods which apply gradient-based search techniques cannot be used. Random search-based GA is used for this problem.

Deb et al.'s [28] elitist non-dominated sorting GA has been used. It is based on elite-preservation and explicit diversity-preservation strategy. Real-coded simulated binary crossover (SBX) [29] and polynomial mutation [30] operators are used for crossover and mutation, respectively. Unlike binary-coded GA, real-coded GA does not need encoding/decoding of real/binary variables. Genetic operators are formulated for real numbered variables. Fitness of the solution is assigned equal to the value of the objective function. Using trial and error, probabilities 0.9 and 0.1 are found to be good for crossover and mutation, respectively. The code is implemented in MATLAB®7.

5.4.1. *Population size and number of generations*

Convergence algorithms for MOGA are not fully established [28]. The convergence of the MOGA involves two main tasks: convergence to PO front and maintenance of a diverse PO set. While these are complex, an idea of convergence can be drawn from the size of elite population in each generation. Elite population is the non-dominated (Front 1) solutions.

Beam with two pairs of collocated piezo S/A is chosen to decide the population and number of generations needed for good converged results. Fig. 4 shows the size of elite population at the end of each generation for population size of 150. It shows the continuous growth in elite population size till 38 generations and after that whole population becomes elite except few occasional drops by 2–3 numbers.

When a better non-dominated solution is discovered, a few existing elite population members may become dominated and hence the size of the elite population decreases. As the elite population size reaches the whole population size and remains constant over generations, it indicates that the probability of the emergence of dominated solutions has reduced and Front 1 reaches to PO front. To find out the population size for minimal

computation cost, various simulations with different population size have been done and population size of 150 has been found to be adequate. For further studies, population size has been taken as 150 except for beam with a single piezo. For those cases, present results are compared with those from exhaustive search study [17], and therefore sufficiently large population (500) has been taken. The results are generated for 100 generations to ensure proper convergence.

6. Optimization results and discussion

Multi-objective GA has been applied to identify the sizing and placement of piezoelectric patches on stationary and rotating cantilever beams. The results are generated for single and multiple piezo patches mounted on the substrate beam. The material properties and geometric parameters of substrate beam and piezoelectric patches used in this study are given in Table 1. While representing the results, length and center of the piezo patch are normalized with respect to length of the substrate beam. The CI is normalized considering maximum value of the controllability as 100 percent. For stationary beam, the NF change is calculated about the corresponding mode frequency of stationary plain beam (i.e. substrate only); while in rotating case, it is calculated with respect to natural frequencies of rotating plain beam. The length of the piezo patches is varied from $0.05L$ to $0.5L$ for the case of beam with a single pair (collocated sensor and actuator) of piezo patches, while for beam with multiple pairs, the total length of piezo actuators on one side of beam is assumed less than or equal to $0.5L$.

To study the effect of the rotation and piezo mounting, the natural frequencies of the stationary plain beam, stationary beam with piezo, rotating plain beam and rotating beam with piezo are compared in Table 2. A cantilever beam of $300 \times 25 \times 0.5$ mm is used for the study. A piezo patch of length 40 mm is mounted on

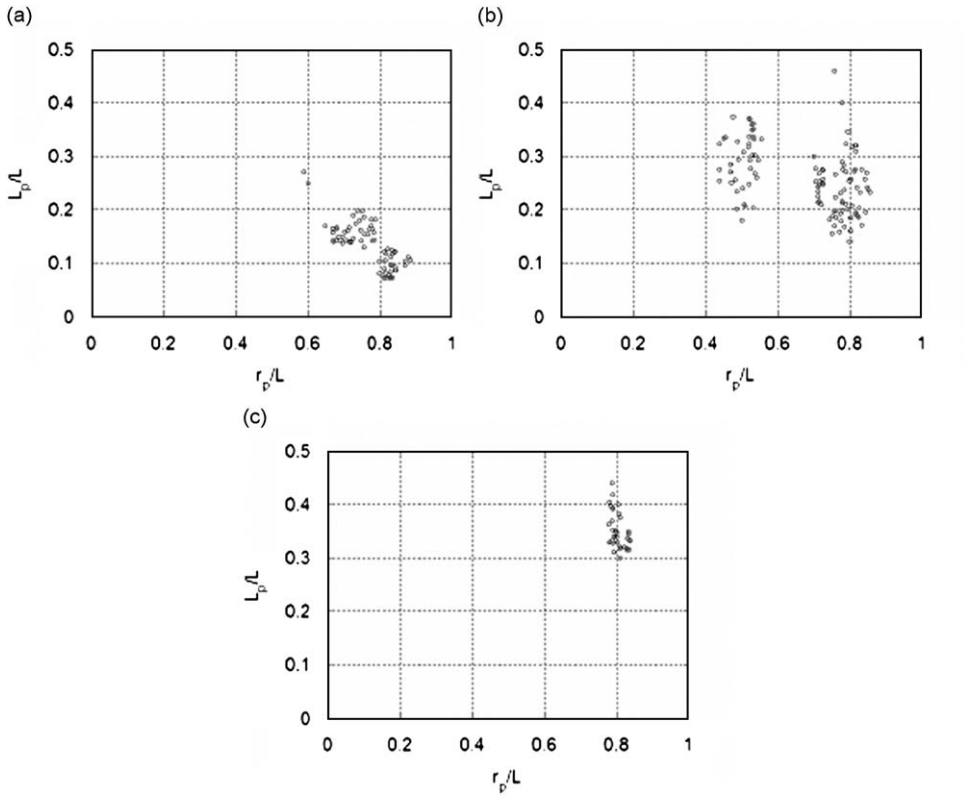

Fig. 12. Pareto optimal solution for rotating ($\Omega/\omega_1 = 0.8$) cantilever beam with a pair of collocated S/A for first four modes: (a) NF change $< 10\%$ and CI $> 20\%$, (b) NF change $< 40\%$ and CI $> 50\%$ and (c) NF change $< 70\%$ and CI $> 90\%$.

the cantilever beam between 210 and 250 mm; the distances being measured from the fixed end. The results from Table 2 show that piezo mounting causes appreciable changes in the dynamics and leads to changes in natural frequencies. The changes (~30 percent) are more for fundamental frequency. Rotation also caused appreciable changes (~57 percent) in the fundamental frequency of plain beam over its stationary value.

6.1. Stationary cantilever beam

The results of individual modal optimal locations are first reported to show that optimal location of one mode be not necessarily optimal for other modes; subsequently optimal sizing/locations are identified considering first four modes together by overlapping their individual modal optimal regions. The results are reported for 1–4 number of piezo patches.

6.1.1. Beam with single piezo actuator

6.1.1.1. Individual modal optimal locations. Fig. 5 gives the PO solutions for first four modes. Fig. 5(a) gives the PO objective set and the Fig. 5(b), the PO solutions. Fig. 5(a) clearly shows that the maximum controllability and minimum NF change are contradictory criteria. Also, NF change is more for fundamental frequency for given control effectiveness among first four modes. From these figures, it can be observed that each individual modal PO solutions give good controllability (CI upto 70 percent) without much change (less than 1 percent) in corresponding natural frequencies. For mode 1, the non-dominated solution is having piezo center (r_p/L) at around 0.4 and normalized piezo length 0.5. The other solutions are patches of length $0.5L$

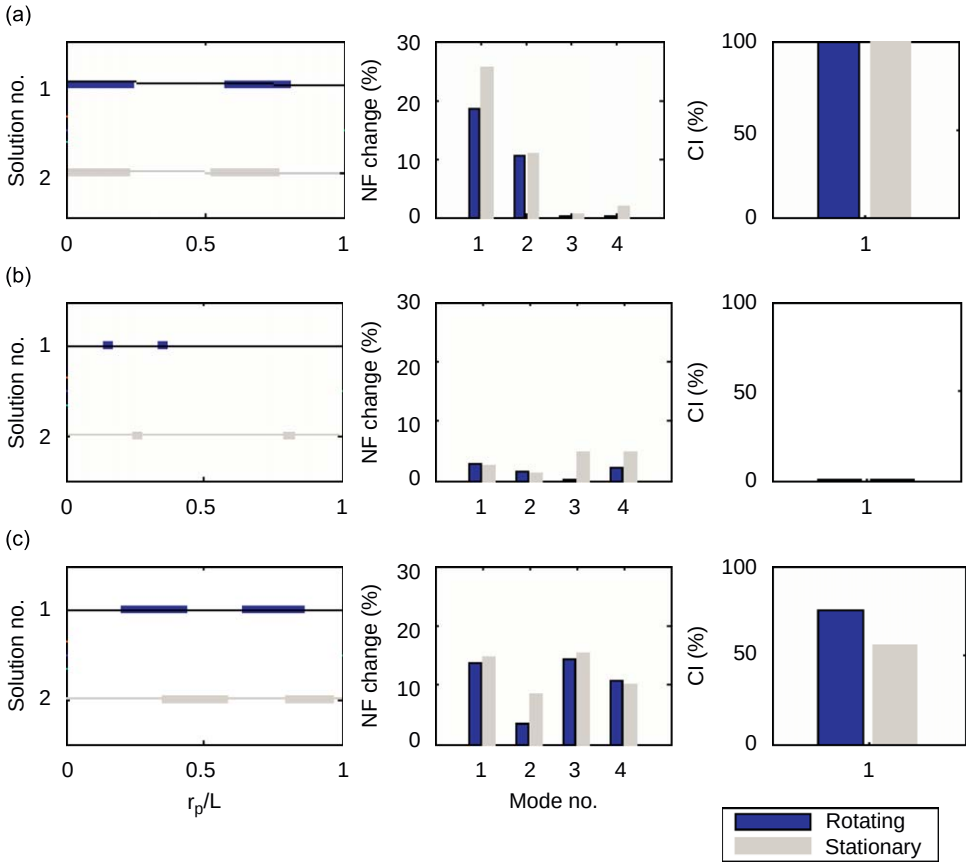

Fig. 13. Comparison of Pareto optimal solutions for a rotating beam with stationary beam, with two piezoelectric actuators: (a) maximum controllability, (b) lesser NF change and (c) CI > 50% with lesser NF change.

mounted between $0.25L$ and $0.4L$ giving controllability more than 74 percent. For mode 2, high controllability (CI > 90%) solutions are piezo patches of length $0.5L$ placed in the region $0.55L$–$0.65L$. Piezos of length $0.35L$–$0.48L$ placed between $0.75L$–$0.85L$ give controllability more than 70 percent for mode 3. Piezo patches having length $0.25L$–$0.35L$ positioned between $0.8L$–$0.85L$ impart controllability more than 75 percent for mode 4. Thus, as we go from modes 2 to 4, for achieving higher controllability, the size of the piezo patch decreases and their position shifts towards free end.

6.1.1.2. Considering all four modes together. The four modes are now considered together to find the optimal locations. The population size has been increased to 500 to have sufficient data points to represent multi-faceted PO surface. Fig. 6 gives the projections of PO objective sets in NF change–CI planes. It is clearly observed that higher controllability can be achieved at the cost of more change in NF.

The results from MOGA are compared with results of our earlier exhaustive search-based study [17] on a beam with a single piezo patch S/A. The PO solutions for different combinations of NF change and CI are plotted in Fig. 7. PO solutions are found to lie within the region identified by exhaustive study. Exhaustive search becomes computationally very intensive for higher number of piezo actuators.

Fig. 8 shows three PO solutions, viz. maximum controllability of all four modes, least change in natural frequencies and, CI > 50% with moderate change in natural frequencies. It is to be noted that the lengths of the piezo patches are not much different for the three cases, but the placement in case of *least NF change* is such that the change in natural frequencies has dropped to less than 3 percent, from an average NF change of 30 percent for *maximum controllability* case. A very good CI (75 percent) is still possible with case-2. In case-3, the CI is 82 percent with an average NF change 9 percent, by slightly increasing the length of piezo patch from $0.37L$ (case-2) to $0.47L$ with almost no change in the center of piezo patch. The length of the piezo patch in

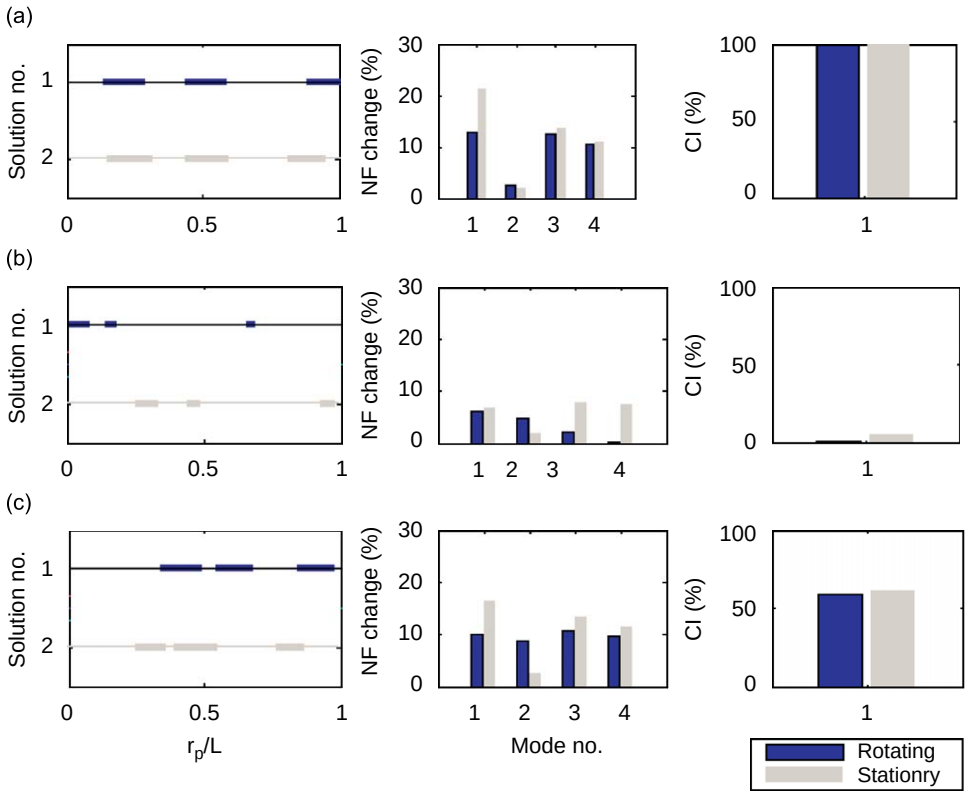

Fig. 14. Comparison of Pareto optimal solutions for a rotating beam with stationary beam, with three piezoelectric actuators: (a) maximum controllability, (b) lesser NF change and (c) CI > 50% with lesser NF change.

first case is 0.42L. Thus, placement of piezo patch i.e. disposition of additional stiffness and mass plays important role in deciding degree of NF change.

6.1.2. Beam with multiple piezo patches

PO solutions have been found for two, three and four piezoelectric patches. PO solutions (actuator placement and sizing) for three different cases, viz. maximum controllability, least NF change and a trade-off solution of former two are given in Figs. 9–11. Some of the observations are: (1) the fundamental frequency change has dropped appreciably (from approximately 50% to 25%) from a single actuator case to multiple actuator case and (2) least NF change is ensured by multiple, short actuators.

6.2. Rotating cantilever beam

6.2.1. Beam with single piezo actuator

The beam is assumed to be rotating at 0.8 times the fundamental frequency. The PO objective sets in various *NF change–controllability* planes resemble those from stationary beam with a single piezo with some minor discrepancies. For a typical speed considered, the NF changes are less for rotating case than for stationary beam. The NF changes depend on the speed of rotation, the size and location of sensors/actuators and relative material properties of substrate and piezoelectric actuators. The PO solutions have been plotted for three different cases in Fig. 12.

6.2.2. Beam with multiple piezo actuator

PO solutions have been found for two, three and four piezoelectric patches mounted on rotating cantilever beam. The beam is assumed to be rotating at 0.8 times the fundamental frequency of stationary beam. The solutions for two extreme cases (i.e. maximum controllability and least changes in the natural frequencies)

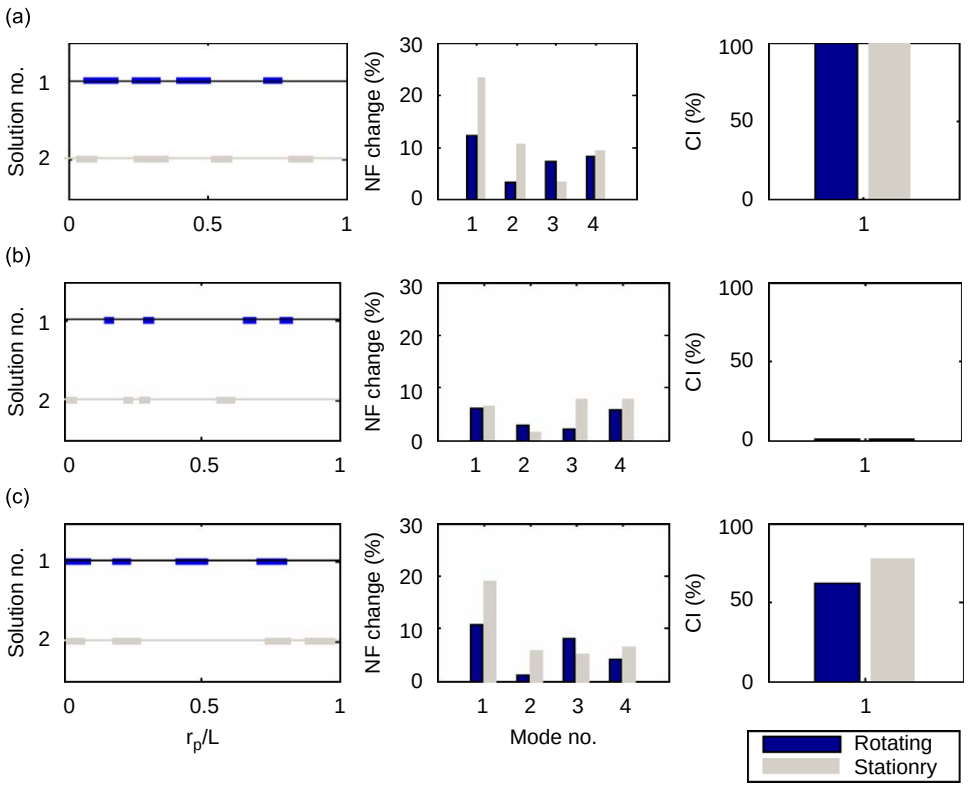

Fig. 15. Comparison of Pareto optimal solutions for a rotating beam with stationary beam, with four piezoelectric actuators: (a) maximum controllability, (b) lesser NF change and (c) CI > 50% with lesser NF change.

and, trade-off of these two are reported in Figs. 13–15. Some of the observations about location, sizing and NF change of rotating case in comparison with stationary are

(1) Just as in the case of stationary beam, shorter piezos do not cause much change in NFs and NF change for fundamental frequency is more than for others.
(2) The piezo actuator locations for maximum controllability are not much changed, while most of the cases, piezo actuator locations for minimum NF change criterion are shifted towards fixed end.
(3) For rotating case, NF changes for most of the modes are smaller compared to those for stationary case. The changes in the natural frequencies are caused due to change in stiffness and inertia due to piezo patches. Rotation causes additional pre-stressing. The effect of pre-stressing due to rotation has been observed to decrease as the locations of the piezo patches shift towards fixed end.

6.3. Active vibration control of cantilever beam using S/A locations based on dynamics and controllability consideration

The performance of the present scheme for optimally locating/sizing piezos is investigated by comparing the active vibration control effectiveness of optimal piezo sizing/location with those for randomly selected piezo sensors/actuators. Simulations have been carried out for two examples: active vibration control of stationary cantilever beam, and active vibration control of rotating cantilever beam.

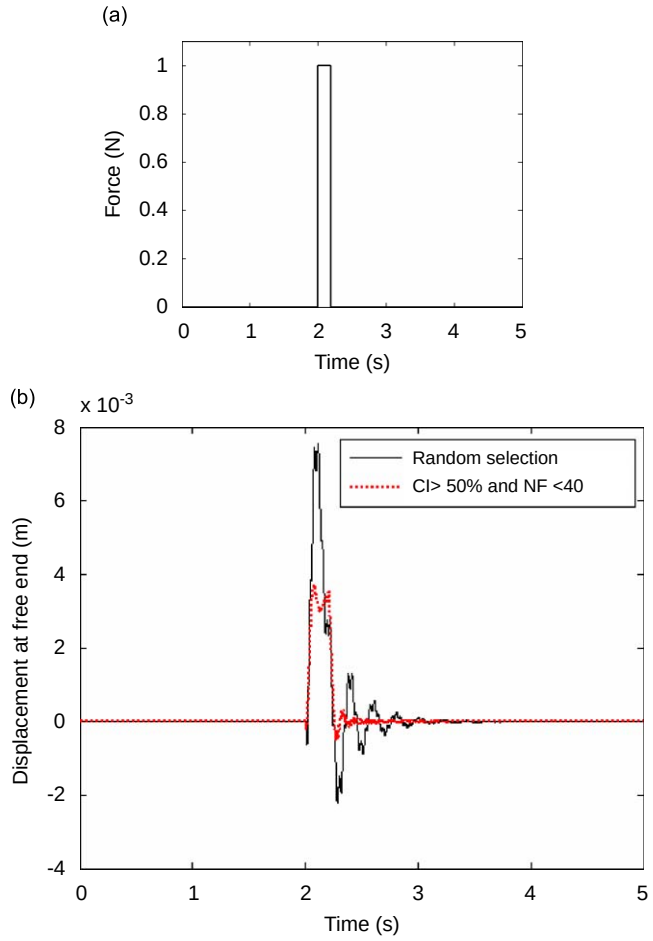

Fig. 16. Force excitation and vibration response of cantilever beam at free end: (a) force excitation and (b) vibration response of cantilever beam at free end.

6.3.1. Active vibration control of stationary cantilever beam

The performance of the location/sizing of piezoelectric S/A, obtained in Section 6.1.1.2, is compared with a randomly selected location of piezo S/A. A solution, $r_p/L = 0.25$ and $L_p/L = 0.18$ from Fig. 7(b) is chosen for the study. Cantilever beam of dimensions $300 \times 25 \times 0.5$ mm is used for the study. The material properties of the cantilever beam and piezoelectric patches are given in Table 1. The locations of the piezo S/A are as follows: trade-off solution (Fig. 7(b)) $\Rightarrow$ 48–102 mm, and randomly selected location $\Rightarrow$ 123–177 mm. The distances are measured from the fixed end of the cantilever beam. Length of the S/A is same for both the cases.

Force excitation as shown in Fig. 16(a) is given at a distance 30 mm from fixed end. PD control has been implemented for vibration control. The gains chosen for the control are: $K_p = 600$ and $K_d = 115$. The vibration at the free end and corresponding active control efforts are shown in Figs. 16(b) and 17, respectively. The NFs of plain beam and beam with piezo S/A are given in Table 3.

From Figs. 16(b) and 17, it can be observed that the control performance is much better for the design based on present scheme (*trade-off of controllability and NF change*) than randomly selected locations for piezo S/As. Considering the first four modes, the CI values for trade-off solution and random selection are 63.27% and 43.21%, respectively, and that is reflected from Figs. 16 and 17.

6.3.2. Active vibration control of rotating cantilever beam

The performance of PO solutions for rotating case is verified by simulating the active vibration control using three collocated sensors/actuators. Sizing and location of piezoelectric sensors/actuators are given in Table 4. The cantilever beam has been rotated using angular velocity profile as shown in Fig. 18(a). Inertia forces set the vibrations. PD control has been implemented for vibration control. Fig. 18(b) gives the comparison of three cases of the PO solution and, one randomly selected design variables (piezo size and location), with uncontrolled vibration response. It can be seen that the vibration is suppressed using active

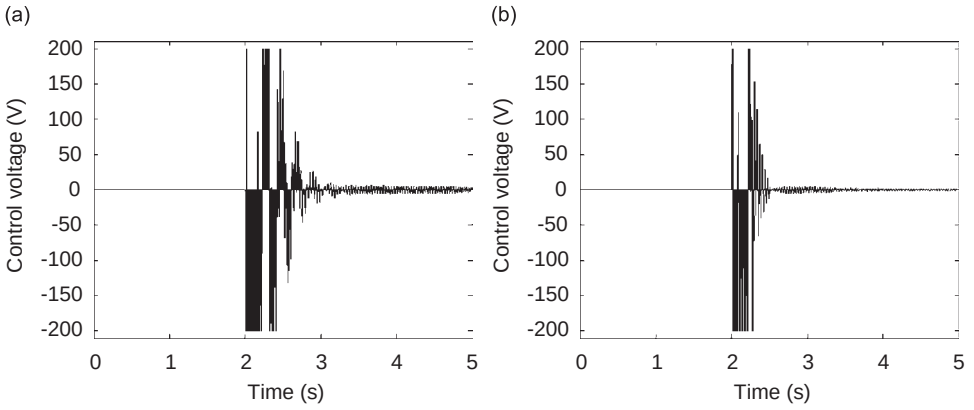

Fig. 17. Control efforts of AVC for: (a) random selection and (b) trade-off solution.

Table 3
Natural frequencies (Hz) of the cantilever beam for different configurations.

Mode number	Plain beam	Random selection	Trade-off solution
1	4.46	3.88 (−13.00)	5.17 (15.92)[a]
2	27.95	25.38 (−9.19)	23.18 (−17.07)
3	78.26	73.44 (−6.16)	71.31 (−8.88)
4	153.36	170.08 (10.9)	153.52 (0.10)

[a]Values in bracket show the % variation in natural frequencies from those of plain beam.

vibration control system. The vibration control using maximum controllability (i.e. CI = 100 percent) gives the best, while min NF change gives the worst control performance. The performance of random selected parameters is better than the minimum NF change solution.

Table 4
Pareto optimal solution with three piezoelectric actuators.

Criteria	Piezo location (r_p) and length (L_p)		
	Patch 1	Patch 2	Patch 3
Maximum controllability	70 (50)[a]	155 (49)	265 (41)
Least NF change	89 (24)	139 (15)	287 (16)
CI > 50% with lesser NF change	91 (35)	141 (48)	246 (31)
Random selection	82 (30)	140 (20)	180 (40)

[a]The values in parenthesis show the piezo-patch length (L_p) in mm.

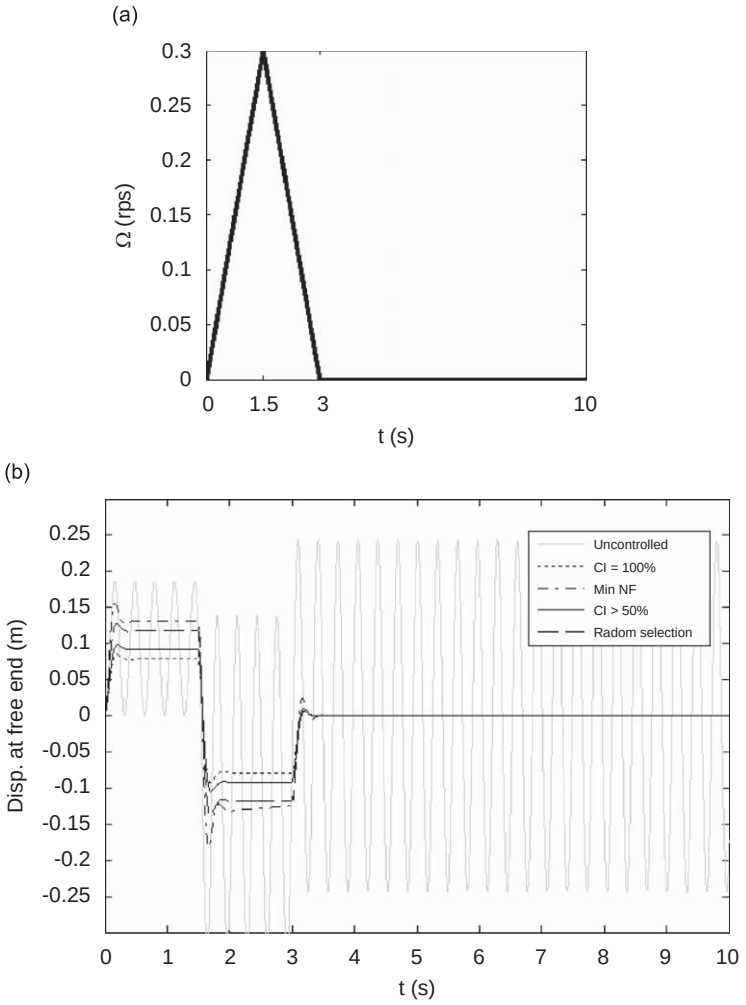

Fig. 18. Speed of rotation (rps) and vibration response of cantilever beam at free end: (a) speed of rotation of cantilever beam and (b) uncontrolled and controlled vibration response.

7. Summary

The study uses multi-objective genetic algorithm (MOGA) to identify the optimal locations and sizing of piezoelectric sensors/actuators. These locations and sizing give good controllability with minimal changes in system natural frequencies. The study has been carried out for stationary and rotating cantilever beam with upto four piezoelectric actuators. Finite element approach has been used for the evaluation of the objective functions (controllability and natural frequency change). Elitist non-dominated sorting GA based on simulated binary crossover and polynomial mutation has been used. PO solutions have been found out for individual modes. The Pareto optimal solutions for three cases, viz. maximum controllability, minimal change in natural frequencies and good trade-off of former two are discussed. Also the performance of the Pareto optimal solution for above three cases is compared with randomly selected solution using active vibration control simulations. The results for beam with a single piezo actuator from MOGA are compared with those from exhaustive search method. Results indicate that the least NF change is obtained using multiple, short piezos. NF change for fundamental frequency is more than for higher frequencies. Also, NF change for fundamental frequency drops appreciably after distributing a single actuator into multiple patches. For rotating case, piezo actuator locations for maximum controllability case are not much changed, but for minimal NF change those are shifted towards fixed end compared to stationary beam.

References

[1] E.F. Crawley, J. de Luis, Use of Piezoelectric actuators as elements of intelligent structures, *AIAA Journal* 25 (1987) 1373–1385.
[2] A. Baz, S. Poh, Performance of an active control system with piezoelectric actuators, *Journal of Sound and Vibration* 126 (1988) 327–343.
[3] S. Devasia, T. Meressi, B. Paden, E. Bayo, Piezoelectric actuator design for vibration suppression: placement and sizing, *Journal of Guidance, Control, and Dynamics* 16 (1993) 859–864.
[4] A.K. Dhingra, B.H. Lee, Optimal placement of actuators in actively controlled structures, *Engineering Optimization* 23 (1994) 99–118.
[5] S.O.R. Moheimani, T. Ryall, Considerations on placement of piezoceramic actuators that are used in structural vibration control, *Proceedings of the 38th Conference on Decision & Control*, Phoenix, AZ, USA, 1999, pp. 1119–1123.
[6] A. Hac, L. Liu, Sensor and actuator location in motion control of flexible structures, *Journal of Sound and Vibration* 167 (1993) 239–261.
[7] Y.K. Kang, H.C. Park, W. Hwang, K.S. Han, Optimal placement of piezoelectric sensor/actuator for vibration control of laminated beams, *AIAA Journal* 34 (9) (1996) 1921–1926.
[8] S.S. Rao, T.S. Pan, V.B. Venkayya, Optimal placement of actuators in actively controlled structures using genetic algorithms, *AIAA Journal* 29 (6) (1991) 942–943.
[9] Y. Yang, Z. Jin, C.K. Soh, Integrated optimal design of vibration control system for smart beams using genetic algorithms, *Journal of Sound and Vibration* 282 (2005) 1293–1307.
[10] L. Sheng, R.K. Kapania, Genetic algorithms for the optimization of piezoelectric actuator locations, *AIAA Journal* 39 (9) (2001) 1818–1822.
[11] A.K. Dhingra, B.H. Lee, Multiobjective design of actively controlled structures using a hybrid optimization method, *International Journal of Numerical Methods in Engineering* 38 (20) (2006) 3383–3401.
[12] L.C. Hau, E.H.K. Fung, D.T.W. Yau, Multi-objective optimization of an active constrained layer damping treatment for vibration control of a rotating flexible arm, *Smart Materials and Structures* 15 (2006) 1758–1766.
[13] Padula, S.L., Kincaid, R.K., *Optimization Strategies for Sensor and Actuator Placement*, Vol. 23681, NASA Langley Research Center, Langley, VA, USA, 1999, pp. 1–12.
[14] M.I. Frecker, Recent advances in optimization of smart structures and actuators, *Journal of Intelligent Material Systems and Structures* 14 (2003) 207–216.
[15] A. Arbel, Controllability measures and actuator placement in oscillatory systems, *International Journal of Control* 33 (1981) 565–574.
[16] S. Kondoh, C. Yatomi, K. lnoue, The positioning of sensors and actuators in the vibration control of flexible systems, *JSME International Journal Series* 3 (33) (1992) 145–152.
[17] K.D. Dhuri, P. Seshu, Piezo actuator placement and sizing for good control effectiveness and minimal change in original system dynamics, *Smart Materials and Structures* 15 (6) (2006) 1661–1672.
[18] R.D. Cook, D.S. Malkus, M.E. Plesha, R.J. Witt, *Concepts and Applications of Finite Element Analysis*, John Wiley & Sons (ASIA) Pte Ltd., Singapore, 2002.
[19] D.A. Turcic, A. Midha, Generalized equations of motion for the dynamic analysis of elastic mechanism systems, *ASME Journal of Dynamic Systems, Measurement, and Control* 106 (4) (1984) 243–248.
[20] K.J. Bathe, *Finite Element Procedures in Engineering Analysis*, Prentice-Hall, Englewood Cliffs, NJ, 1982.

[21] S. Burke, J. Hubbard Jr., Active vibration control of a simply supported beam using a spatially distributed actuator, *IEEE Control Systems Magazine* 7 (4) (1987) 25–30.
[22] S.B. Choi, H.C. Shin, A hybrid actuator scheme for robust position control of a flexible single link manipulator, *Journal of Robotic Systems* 13 (6) (1996) 359–370.
[23] J. Thomas, C.A. Mota Soares, Finite element analysis of rotating shells, ASME Paper, No. 73-DET-94, 1973.
[24] MATLAB®7.0, The MathWorks, Inc., MA, USA.
[25] S. Miller, J. Habbard Jr., Observability of a Bernoulli–Euler beam using PVF2 as a distributed sensor, *Proceedings of the Seventh Conference on Dynamics and Control of Large Structures*, VPI and SU, Blacksburg, VA, May 1987, pp. 375–390.
[26] Q. Wang, C.M. Wang, Optimal placement and size of the piezoelectric patches on beams from the controllability perspective, *Smart Materials and Structures* 9 (4) (2000) 558–567.
[27] K. Deb, *Multi-Objective Optimization Using Evolutionary Algorithms*, Wiley, Chichester, UK, 2002.
[28] K. Deb, A. Pratap, S. Agarwal, T. Meyarivan, A fast elitist multiobjective genetic algorithm: NSGA-II, *IEEE Transactions on Evolutionary Computation* 6 (2) (2002) 182–197.
[29] K. Deb, A. Kumar, Real-coded genetic algorithms with simulated binary crossover: studies on multimodal and multi-objective problems, *Complex Systems* 9 (6) (1995) 431–454.
[30] K. Deb, M. Goyal, A combined genetic adaptive search (GeneAS) for engineering design, *Computer Science and Informatics* 26 (4) (1996) 30–45.
[31] Sparkler Ceramics Pvt. Ltd., Pune, India 〈www.sparklerceramics.com/mat3.html〉.